CHALMERS

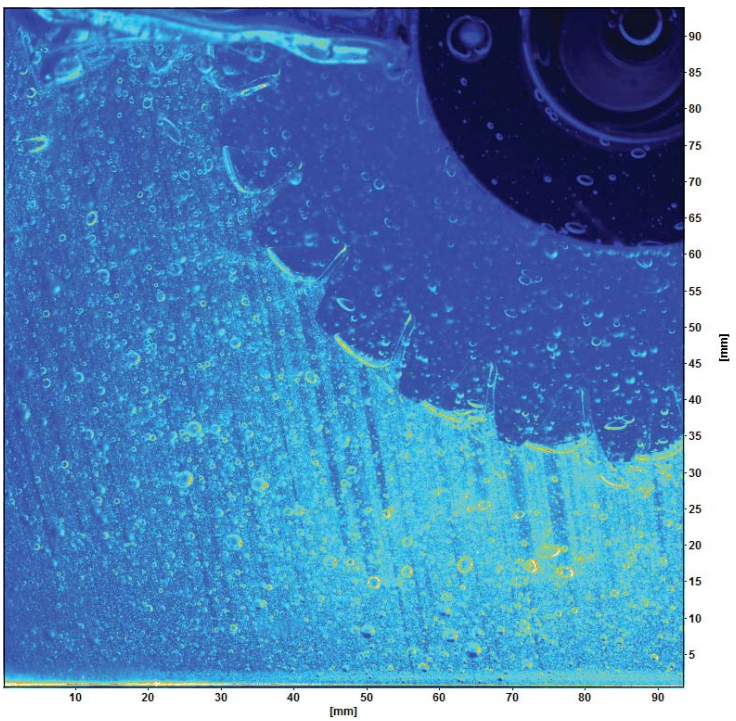

Study of Fluid Flow Inside The Gearbox

ERWIN ADI HARTONO

Department of Applied Mechanics
Division of Fluid Dynamics
CHALMERS UNIVERSITY OF TECHNOLOGY
Gothenburg, Sweden 2014

THESIS FOR THE DEGREE OF LICENTIATE OF ENGINEERING IN THERMAL AND FLUID DYNAMICS

Study of Fluid Flow Inside The Gearbox

ERWIN ADI HARTONO

Department of Applied Mechanics
Division of Fluid Dynamics
CHALMERS UNIVERSITY OF TECHNOLOGY
Gothenburg, Sweden 2014

Study of Fluid Flow Inside The Gearbox
ERWIN ADI HARTONO

Thesis for the degree of Licentiate of Engineering 2014:12
ISSN 1652-8565
Department of Applied Mechanics
Division of Fluid Dynamics
Chalmers University of Technology
SE-412 96 Gothenburg
Sweden
Telephone: +46 (0)31-772 1000

Cover:
Raw image from planar PIV measurement

Chalmers Reproservice
Gothenburg, Sweden 2014

Study of Fluid Flow Inside The Gearbox
Thesis for the degree of Licentiate of Engineering in Thermal and Fluid Dynamics
ERWIN ADI HARTONO
Department of Applied Mechanics
Division of Fluid Dynamics
Chalmers University of Technology

Abstract

Long haul trucks spend (almost) 80% of their time cruising from one destination to another. This means that they drive mostly at a constant speed and use their top gear most of the time. Depending on the gearbox, the top gear of long haul trucks is usually direct drive gear. With the direct drive gear losses mainly come from the interaction between lubricant and rotating gear (churning losses). It is obvious that using a small amount of low viscosity lubricant will reduce the churning losses dramatically. Unfortunately the solution is not as simple as that. This is because, besides lubrication, the lubricant is also there as a cooling agent. Hence, too little oil will affect the heat dissipation and the lifetime of the gear. Studies of oil flow inside the gearbox are needed to find ways to reduce churning losses and good heat dissipation.

A simplified version of a gearbox is built to study the flow, due to the complexity of the real gearbox. The new gearbox consists of a gear pair and has transparent rectangular walls to ensure good optical access. Velocity measurements with particle image velocimetry (PIV) are made to get the velocity field around the gear. Flash photography is done, as additional data, to study the flow distribution. Finally, torque measurements are made to measure the losses.

It was found in the PIV study that oil flow is dominated by a recirculation region. The recirculation is suspected to be the source of viscous losses. The oil flow inside the gearbox is highly three dimensional. Stereo-PIV has successfully revealed the third components of the flow. PIV measurements also reveal that the squeezing of the oil at the gear contact is considered minor compare to the losses due to recirculation. From flash photography, the splash pattern and oil distribution is studied. The oil distribution inside the gearbox is governed by a gear with a larger diameter. The larger diameter gear splashes more oil compared to the smaller one. This is most probably because the larger diameter gear is more immersed compared to the smaller diameter gear. Hence, the larger diameter gear drags more oil upward. Torque measurements show that the torque is dependent on the rotational speed, the immersion depth, and the oil properties. The oil properties are suspected to be changed when the oil is aerated, resulting in a higher torque reading.

Keywords: PIV, gearbox, lubrication, oil, flow

If you want it... You must will it...
If you will it... It will be yours...

- The Mighty Sven

Preface

This licentiate text is a report about my work during two and a half years of my studies as a PhD student at Chalmers University of Technology. It covers the experimental part of fluid flow in a study inside the gearbox, from fluid flow visualization to the state of the art laser measurement technique, PIV (Particle Image Velocimetry). Brief theories about gearbox lubrication and PIV have also been given. Torque measurement is also reported to complete the analysis of the fluid flow inside the gearbox. One is encouraged to read in an orderly way from Chapter 1, since all the backgrounds and necessary theories are presented in the beginning of the report.

Acknowledgements

Thanks to the Fluid Dynamics Division, Applied Mechanics Department, Chalmers University of Technology, where this research has been conducted. Thanks to all the professors, researchers, teachers, students and staff at the Fluid Dynamics Division. Special thanks to my supervisor, Valery Chernoray, and my co-supervisor, Håkan Nilsson, for teaching and guiding me to do research work since I was a Master Student.

Thanks to FFI (Fordonsstrategisk Forskning och Innovation) and all the members of it. Special thanks to Lennart Johansson, AB Volvo; Mårten Dahlbäck, Scania, Martin Andersson, KTH. Also thanks to Usman Afridi, Vicura AB for collaboration and input.

Finally I thank God, my family, all of my friends, and all other people that have helped me.

Thesis

This thesis consists of an extended summary and the following appended papers:

Paper A E. A. Hartono, M. Golubev, and V. Chernoray. "PIV Study of Fluid Flow inside a Gearbox". In: *Proc. of 10th International Symposium on Particle Image Velocimetry* (2013), pp. 1–11

Paper B E. A. Hartono, A. Pavlenko, and V. Chernoray. "Stereo-PIV Study of Oil Flow inside a Model Gearbox". In: *Proc. of 17th International Symposium on Applications of Laser Techniques to Fluid Mechanics* (2014), pp. 1–8

Contents

Part I
Extended Summary

1 Introduction

1.1 Background

Heavy duty vehicles, such as trucks and buses, are the backbone of our society. This is because heavy duty vehicles are used for mass transportation of people, products and services. Unfortunately, the fuel economy and carbon footprint of heavy duty vehicles are quite bad [1]. Only 34% of fuel energy is converted to move the vehicles. The rest is used for cooling (20%), exhaust (30%), engine (7.3%), transmission (5.1%), and others (3.6%). Figure 1.1.1 shows the breakdown of heavy duty vehicles' energy consumption.

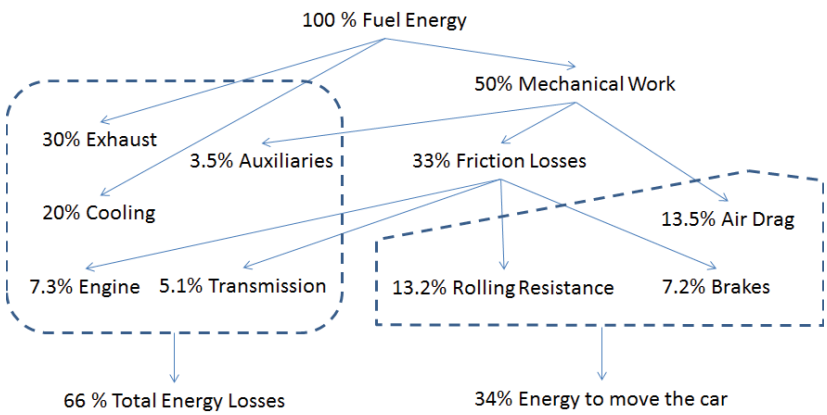

Figure 1.1.1: *Breakdown of energy consumption for the global fleet of trucks and buses [1]*

Nowadays efforts to make energy efficient vehicles are not only for economic but also for environmental reasons, which is to meet the requirement of CO_2 emissions by the Kyoto protocol on climate change. The CO_2 emissions produced by road transports account for more than 80% of the total 18% of the total anthropogenic greenhouse gas emissions [2]. Another environmental problem comes from the use of mineral oil as lubricant, due to the disposal problem. Even though the base oils are biodegradable in the long run, the presence of additives in the finished lubricants makes them poorly compatible with the ecosystem.

1.2 Purpose

Improvement of the efficiency of heavy duty vehicles is quite challenging, since the power-to-weight ratio of the heavy duty vehicles is quite different from passenger cars. A significant fuel saving can be achieved by downsizing the engine of passenger cars, but the same method will not work in heavy duty vehicles [1]. Hence, an alternative solution for increasing fuel efficiency needs to be found.

A significant reduction of losses can be achieved, if the marginal efficiency gain from each component in the vehicle is considered. For long haul trucks using a splash lubrication system, viscous losses are one of the major sources of power loss. This is because they spend almost 80% of the time cruising. When cruising, the gearbox is usually in direct drive gear. At direct drive, the contribution to losses due to load on the gear is small and the losses mainly come from viscous losses [3]. The obvious way to reduce the viscous losses is to use low viscosity oil. By switching to a lower viscosity lubricant (oil), the potential saving of fuel can be up to 2.5% [1], but low viscosity oil has detrimental effects on surface durability [4]. Minimizing the oil volume inside the gearbox can also further reduce the viscous losses, but the lifetime of the gear will be affected due to less heat dissipation, as suggested by [5], [6], and [7]. Spray lubrication is also a possible solution to reducing viscous losses, but an additional device in the system means additional energy and complexity that needs to be addressed. Finding ways to have good heat dissipation, good lubrication, and low energy losses is a challenge the in development of new gearboxes. Hence, further studies of oil flow inside a gearbox are needed as a first step to reduce the viscous losses.

1.3 Limitation

The complete gearbox system is beyond the scope of this study, since the point of interest here is to understand the interaction between the gear and the oil and how the oil flows. Hence, the study is limited to a simplified gearbox in the form of a rectangular box with a spur gear pair inside. The gearbox and the test gear design are based on the standardized test rig (FZG back to back gear test rig). The maximum pitch line velocity is limited by the maximum rotational speed of the motor, which is 2980 RPM. For a pair of FZG gear type C, 2980 RPM corresponds to 18.84 m/s pitch line velocity.

1.4 Scope of this work

Oil flow inside a gearbox is very chaotic, especially in high rotational speed. The real gearbox with all its components and tight space are not a suitable platform for studying the oil flow inside a gearbox. Therefore a simplify version of the real gearbox is needed for this study. The FZG back to back test rig is used as a basis for the new experimental rig. This is because the FZG test rig is a standardized test rig and has quite simple components. It has a gear pair and a rectangular box. The Chalmers gearbox test rig utilizes the same layout as the FZG test rig and modifies it for fluid dynamics study. Details on the rig can be found in Chapter 2.

A state of the art measurement technique called Particle Image Velocimetry (PIV) is used to measure the flow velocity inside the gearbox. PIV utilizes particles as a tool to measure flow velocity. More detail on PIV in this study can be found in Chapter 4. Flow visualization with flash photography was used to visualize the splash, to study the distribution and to gain further understanding about phenomena that occur with the oil when the gear is rotating at different rotational speeds. Chapter 6 gives details on the flow visualization in the present study.

The amount of torque that is needed to rotate a gear immersed in a lubricant will determine the viscous losses in the gearbox. Obviously, the least amount of torque needed for turning the gear is desired, but the requirement for cooling limits the amount of oil inside the gearbox. Therefore it is essential to study the torque measurements. The torque measurements made are reported in Chapter 5.

All the results from flow visualization, PIV, and torque measurements are used as additional knowledge and also as a database for validating numerical results in future studies.

2 Experimental Apparatus

2.1 Chalmers Gearbox Flow Facility

The Chalmers Gearbox flow facility (the Chalmers rig) is a new facility at the Fluid Dynamics Division, Chalmers University of Technology. It was designed and built for studying fluid flow inside a gearbox by using optical measurement techniques. The design is based on the FZG (*Forschungsstelle fur Zahnrader und Getriebebau*) test rig with some modifications to accommodate the need of optical measurement. There are some parts that are different from the FZG test rig due to the different purposes of the rig. The test section and the gears in the Chalmers rig are made of PMMA (acrylic glass). PMMA is chosen due to the optical properties. The limitation of using PMMA is that the temperature inside the test section is limited to the forming temperature of PMMA ($\sim$ 100°C) [8]. The loading arm in the FZG test rig is not present in the Chalmers rig. This is because the focus of the current study is to investigate the gearbox from a fluid dynamics perspective. Hence, additional loads that do not come from the fluid are eliminated. The gear contact is also eliminated. The FZG gear and the FZG pinion are driven by a drive belt, since the load comes only from oil inside the test section, and this is relatively small. As a result of simplification, the Chalmers rig is much lighter than the FZG test rig. Hence, detailed calculations for structural strength and vibration of the Chalmers rig can be negligible and the rig can be built and mounted on a 15 mm thick aluminium slab. Figure 2.1.1 shows the schematics of the Chalmers rig and the FZG test rig.

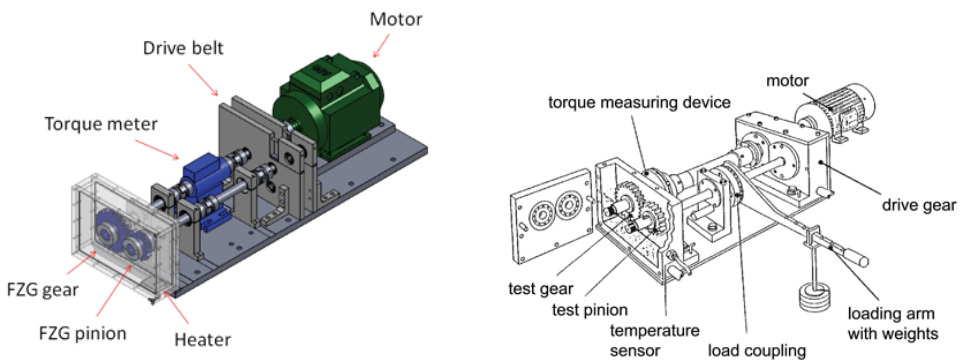

(a) *The Chalmers rig* (b) *The FZG test rig*

Figure 2.1.1: *The schematic of The Chalmers Rig and the FZG test rig*

The Chalmers rig test section wall is made of 15 mm PMMA. Figure 2.1.2 shows a closer look at the test section. The inner dimension of the test section is $269 \times 180 \times 56[mm^3]$. It is equipped with a pump, a draining hole, and a breathing hole for easy refilling or reducing the oil level inside the test section. It also has a heater embedded inside the bottom wall of the test section in order to control the oil temperature. The heater is automatically driven by feedback from a temperature sensor embedded in the heater. A

thermocouple is inserted via a breathing hole to measure the bulk temperature of the oil.

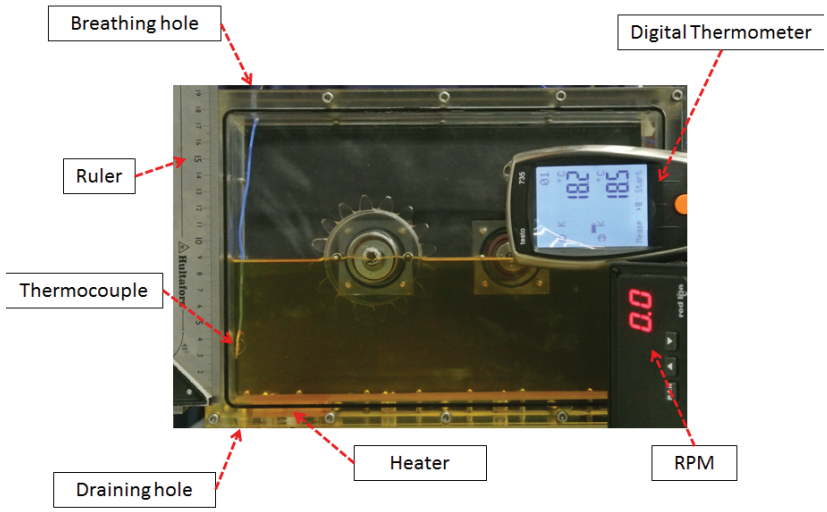

Figure 2.1.2: *The Chalmers rig test section*

Two pairs of gears are studied. One is based on the FZG type C gear pair and the second pair is a cylinder. Figure 2.1.3 shows the gears and cylinders studied. Table 2.1.1 shows the specification of the gears and the cylinders.

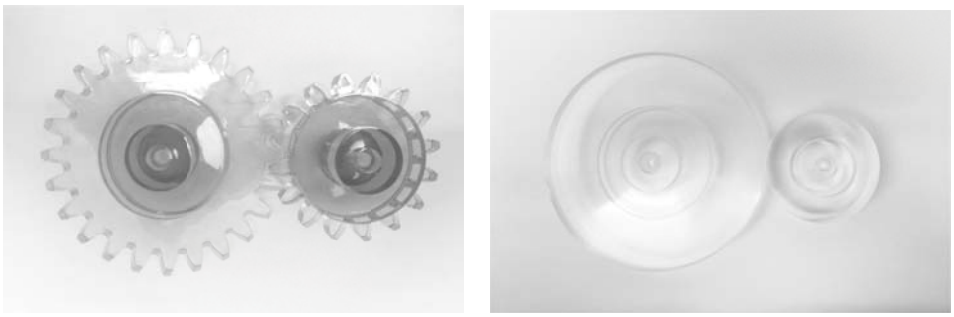

(a) *FZG gear (big) and FZG pinion (small)*

(b) *Cylinder gear (big) and Cylinder pinion (small)*

Figure 2.1.3: *The gears and pinions in this study*

2.2 Test Oil

Napthenic base oil (Nytex 810) is used as a test oil due to its transparent appearance and the refractive index matching that is close to PMMA. With those two requirements

Parameter	Unit	FZG Gear	FZG Pinion	Cylinder Gear	Cylinder Pinion
Number of teeth	-	24	16	-	-
Module	mm	4.5	4.5	-	-
Centre distance	mm	91.5	91.5	91.5	91.5
Face width	mm	14	14	14	14
Tip diameter	mm	118.4	82.5	120	60
Pitch diameter	mm	109.8	73.2	-	-

Table 2.1.1: Dimension of the gears and the cylinders

fulfilled, good optical access is ensured. Table 2.2.1 shows the properties of the test oil. Figure 4.1.5, in Chapter 4, shows the refractive index match between the test oil and the PMMA.

Property	Unit	Data
Density, 15°C	kg/cm^3	901
Viscosity, 40°C	cSt	22.4
Viscosity, 100°C	cSt	3.7
Refractive index, 20°C	-	1.493
Appearance	-	clear

Table 2.2.1: Properties of test oil

3 Lubrication in a Gearbox

3.1 Lubricant Function

The main function of a lubricant / oil is to prevent metal to metal contact (reduce friction) by creating a thin film of oil surrounding the surfaces. Other important functions of the lubricant in a gearbox besides reducing friction according to [9] are:

1. Heat dissipation
   In a gearbox, after gear teeth meshing / engaging / in contact, the teeth temperature will rise. This is because friction creates heat. The oil inside the gearbox can act as a cooling agent to transfer the heat from the gears to the surroundings.

2. Carry out contamination
   External contamination can be controlled by filters, seals, and other control units, but it is impossible to completely eliminate machinery wear. These wear particles, if they are not removed from the surfaces, can act as an abrasive agent and create more wear. Oil can suspend them and transfer them into the filter, where they will be removed.

3. Avoid corrosion
   Corrosion on metal / alloy is due to exposure to moisture. Oil can prevent metal from coming into contact with water, which prevents the production of rust, and therefore prevents corrosion.

4. Solve additives
   For any given oil, the ingredients are base oil and additives. There are many additives that can be added into the base oil to alter its properties for a particular usage. Some examples of additives are: rust inhibitors, dispersant, detergents, defoamants, and many more.

3.2 Viscosity

The most important parameter to consider when selecting a lubricant / oil is its viscosity [10]. Depending on the load and the speed of the system, the viscosity of the lubricant / oil has to be chosen accordingly so that metal to metal contact can be avoided.

It was previously necessary to change the vehicle oil according to the season. A thinner oil was needed in the winter and a thicker oil in the summer. This is because low temperature increases the viscosity of the oil, which can create trouble when starting the engine due to a high load. For high temperature, the viscosity of oil is low, and a thicker oil is needed so that it can still provide an oil cushion for contact. Fortunately, nowadays oil comes with multi-grade, so that the oil can adjust itself to the temperature.

3.3 Lubrication System

There are three types of lubrication systems based on the rotational speed; grease lubrication for low rotational speed, splash / dip lubrication for medium, and force feed for high rotational speed. A complete presentation of the systems and guidelines for how to select a lubrication system can be found in [11] section C.13. Figure 3.3.1 shows a schematic of a 1996 Land Rover Discovery Manual Gearbox. Each part has been labelled with a number. A description of each number is given below. Arrows in the figure indicate the flow of the oil through a filter, then the pump, and then into the main shaft for lubricating the bearings. In some trucks the oil can be pumped outside the gearbox for extra cooling before re-entering the gearbox to lubricate the bearings.

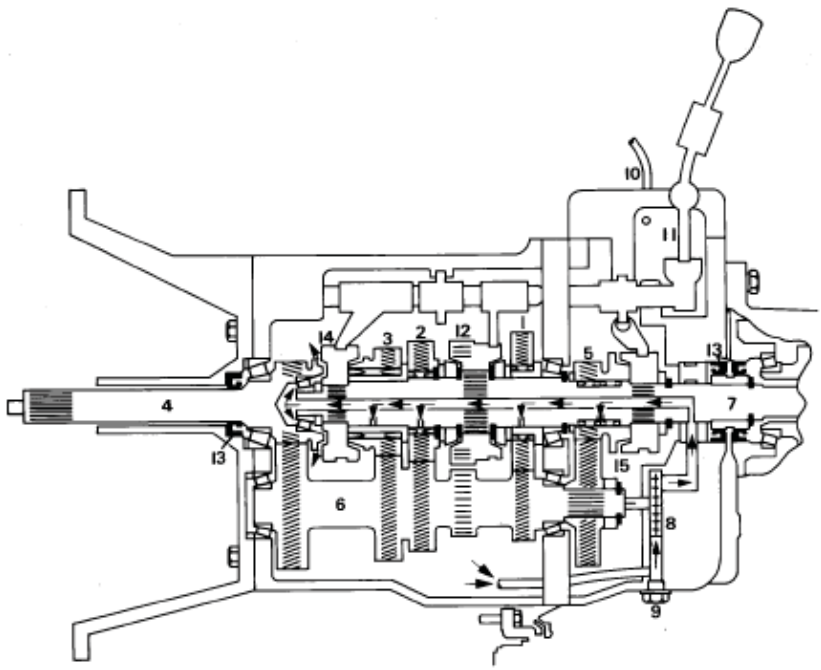

Figure 3.3.1: *Assembly of 1996 Land Rover Discovery Manual Gearbox [12]*

1. Mainshaft 1st gear
2. Mainshaft 2nd gear
3. Mainshaft 3rd gear
4. Primary input shaft
5. Mainshaft 5th gear
6. Counter shaft
7. Mainshaft
8. Lubrication pump
9. Drain plug
10. Ventilation pipe
11. Shift lever
12. 1st/2nd synchromesh
13. Oil seals
14. 3rd/4th synchromesh
15. 5th gear synchromesh

This study evaluates a splash / dip lubrication system. As the name suggests, a splash / dip lubrication system means that the gears are partially immersed in an oil bath and, when the gears rotate, they will splash oil to the surroundings and some of the splash will lubricate other parts inside the gearbox. In a splash / dip lubrication system, the large amount of oil is beneficial for removing the heat from the gear teeth. A large amount of oil also keeps the rate of oil circulation low, allowing any impurities to settle down and be filtered. The drawbacks of splash / dip lubrication system are the lack of control of the lubrication supply [13] and the large oil level that must be maintained, which leads to high churning losses [14].

In cars / trucks gearbox, the lubrication system is usually a combination between splash lubrication and force feed lubrication. As rotational speed or load requirement is higher, the needs of lubrication and cooling increase. Force feed lubrication is added to assist bearings and other components lubrication in the gearbox.

4 Particle Image Velocimetry (PIV)

This section gives a brief explanation of PIV. For more detail and a thorough explanation of the PIV technique, see [15], [16], [17], [18] and [19].

4.1 Basic Knowledge

Particle Image Velocimetry (PIV) is an indirect measurement technique of fluid flow velocity. It records and analyses the displacement of particles immersed in the fluid flow itself. The displacement of the particles is recorded photographically. At least two consecutive images, with a known time interval (Δt), are needed in order to be able to determine the displacement of the particles (Δx). The velocity is then calculated by computing the displacement of the particles over a given time interval. The time interval should be small enough so that the mean particle shift is about 5 pixels and the maximum particle image shift should be less than a quarter of the interrogation window size [20]. Laser is chosen and widely used since it can emit high energy density monochromatic light when illuminating the particles, and hence there is no chromatic aberration in the recording [19].

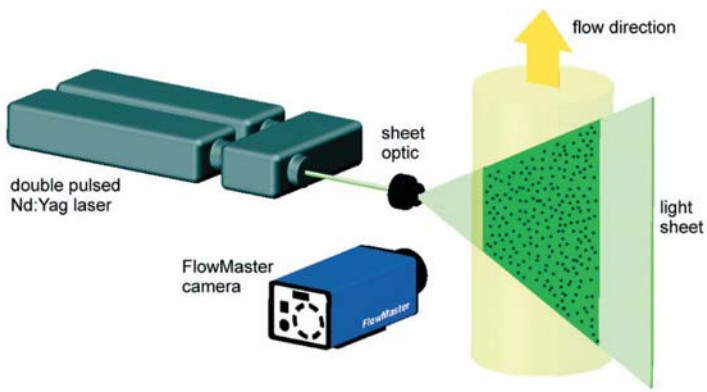

Figure 4.1.1: *Schematic of PIV setup. [21]*

The displacement is derived from analysing the intensity (I) of image pairs using a statistical approach based on localized interrogation windows [19]. As seen in Figure 4.1.2, the process starts with dividing images 1 and 2 into a large number of sub-areas called interrogation windows. The spatial correlation between the two interrogation windows is calculated using the discrete Fourier transform, which can be computed efficiently using the fast Fourier transform (FFT). Hence, the FFT (Fast Fourier Transform) operation is done on each of interrogation windows in images 1 and 2 individually. The cross correlation in the spatial frequency domain (R_{II}) is then done for each pair of interrogation windows

between images 1 and 2.

$$R_{II} = \hat{I}_1 \cdot \hat{I}_2{}^{\prime *} \tag{4.1.1}$$

Inverse FFT is done to calculate the cross correlation peak detection. The peak corresponds most likely to the displacement of particles ensemble in the interrogation window [22]. Conversion to the velocity field is done by dividing the displacement vector by the time interval.

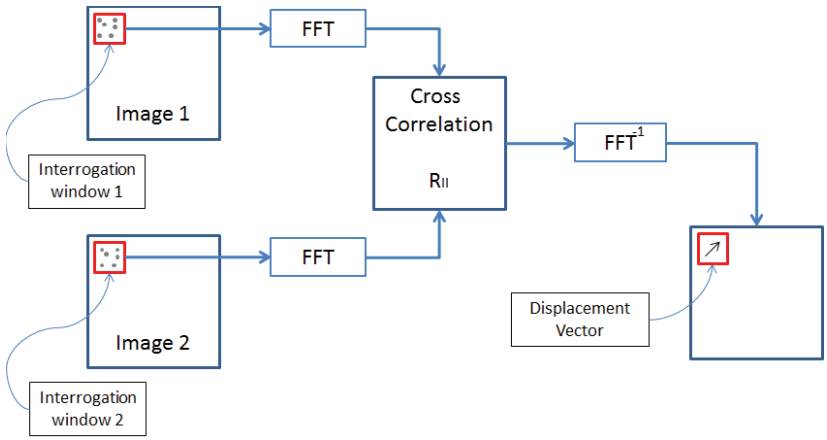

Figure 4.1.2: *PIV algorithm flow chart*

Seeding

The seeding / tracer particles are critical in the PIV measurement since the fluid velocity is measured via the particles velocity. The first consideration when choosing the seeding particles is therefore visibility [18]. The particles have to have a sufficient size and a good refractive index in order to achieve good scattering intensity. The size of the particles must be balanced with the fidelity of the particles following the flow. For acceptable tracing accuracy, the particle response time should be faster than the smallest time scale of the flow. The accuracy of the PIV measurement is therefore limited by the ability of the tracer particle to follow the fluid flow [23].

The non-dimensional number that measures the faithfulness with which the particle follows the flow is the Stokes number. The Stokes number is defined as the ratio of the response time of a particle to a response time of the flow. The condition where $St < 0.1$ gives an acceptable flow tracing accuracy with errors of less than 1% [24]. Figure 4.1.3 gives an illustration of the Stokes number effect.

Another important aspect of seeding is the quantity of the seeding inside the system. The volume fraction of the particles inside the fluid should not change the viscosity of the fluid. An example of ten particles of a diameter of 20 μm in a cubic interrogation volume 500 μm is a good measure [18].

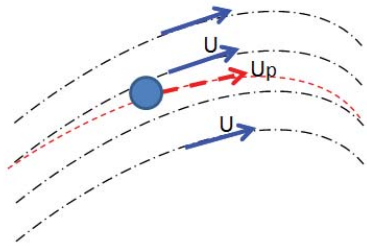

Figure 4.1.3: *Illustration of Stokes number. Velocity discrepancy between particle and the surrounding fluid velocity [24].*

In this study, the rotational speed of the gears entrains air into the oil and creates a great deal of bubbles. Although these bubbles can become a natural seeder for the flow, the bubbles in this study are not used as seeders. This is because these bubbles come in a variety of sizes and only the small bubbles that faithfully follow the flow. Therefore, the bubbles are considered unreliable for use as a seeder in this study. Instead of using bubbles, the fluorescent particles (Rhodamine B) are used in this study. The fluorescent dye absorbs the incident light (Nd:YAG laser 532 nm) and this light is re-emitted at longer wavelengths (550-680 nm) [24]. The fluorescent particles are used in combination with an optical filter that removes the scattering from other objects (walls, bubbles, other particles) in the flow and only allow a certain wavelength (the tracer particles, Rhodamine B) to pass through. Figure 4.1.4 shows a comparison of the quality of the image with and without fluorescent particles.

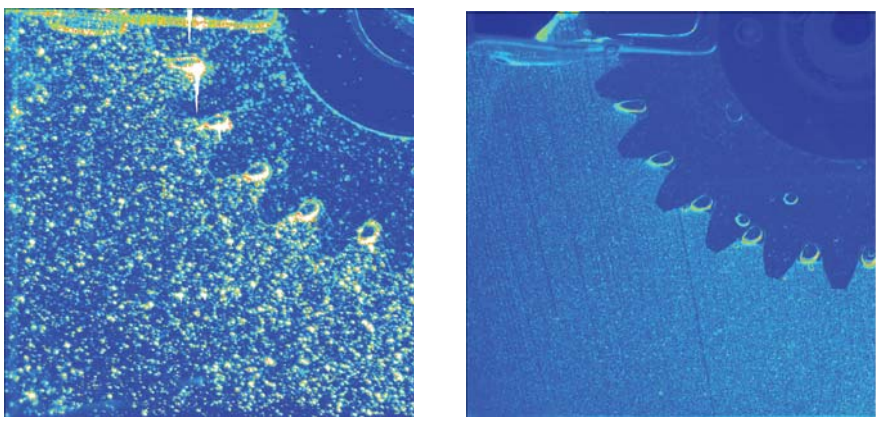

(a) *Air bubbles used as tracers* (b) *Fluorescent particles used as tracers*

Figure 4.1.4: *Comparison of PIV raw image with different tracers. Note that the bright spot is a result of light reflected by the bubbles and the walls are reduced significantly.*

Refractive Index Matching

The refractive index matching ensures that the light that shines through the body in the liquid will not create refraction that can disturb the measurement region [22]. Figure 4.1.5 shows the refractive index matching between PMMA (1.4914) and hydro-treated process oil (1.494).

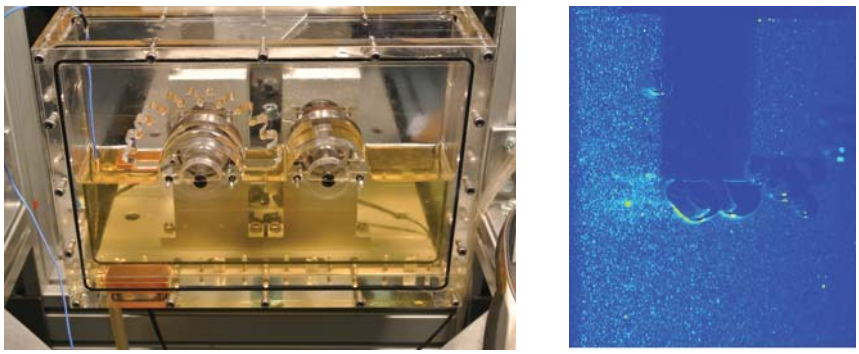

(a) *Image from ordinary camera* (b) *Image from PIV camera*

Figure 4.1.5: *Refractive index matching. Note the outline of the gear seems to disappear.*

4.2 Types of PIV

There are many types of PIV, such as:

- 2D-2C PIV
- 2D-3C (Stereo) PIV
- 3D-3C (Tomographic) PIV
- Micro PIV
- Ultrasound PIV, and many more

2D-2C PIV (Two Dimensional - Two Components PIV) and 2D-3C (Stereo) PIV (Two Dimensional - Three Components PIV) are used for this study. 2D-2C PIV utilizes one camera and a laser sheet for measurement. The resulting data would be two dimensional and two components velocity fields. Stereo PIV also use planar light, but now the third (out-of-plane) component of the velocity can be reconstructed due to the stereoscopic arrangement. Tomographic PIV or 3D-3C PIV (Three Dimensional - Three Components PIV) is suitable for use for three dimensional and three component velocity measurements. Micro PIV is suitable for microfluidics flow. And Ultrasound PIV is suitable for measurements in non-transparent objects / fluids.

4.2.1 Stereo-PIV

Planar PIV can only extract two velocity components due to the nature of photographic recording, which can only capture the projection of the real image in a two dimensional plane. For highly three dimensional flow, this limitation can lead to substantial measurement errors [19]. The out-of-plane component is lost and the measured in-plane vectors are contaminated with perspective errors as a result of a local non zero out-of-plane component [25]. The most straightforward method for extracting the third velocity component is to add a second camera (stereoscopic recording) [26]. The arrangement of the camera can vary depending on the optical access and the region of interest. The most common arrangement is two cameras symmetrically aligned at about a 45-degree displacement angle while enforcing the Scheimpflug condition. The displacement angle of 45 degrees gives the smallest error ratio between the in-plane error and out-of-plane error [27]. Figure 4.2.1 shows the schematic of the common stereo-PIV set-up with an angle displacement arrangement using the Scheimpflug condition.

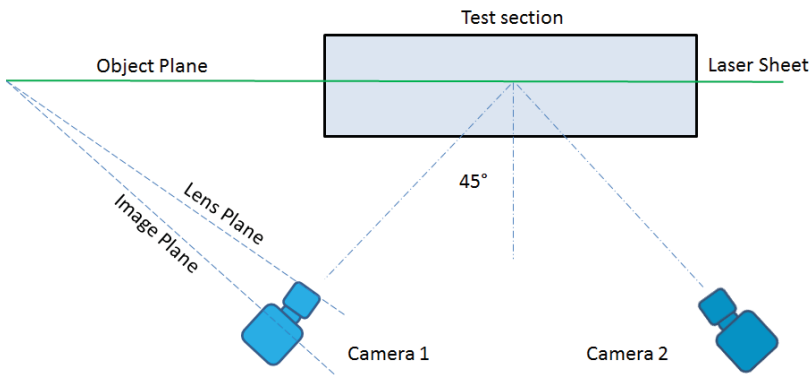

Figure 4.2.1: *Stereo PIV setup with an angle displacement arrangement using the Scheimpflug condition. The Scheimpflug condition is a condition where the film plane, lens plane and focus plane intersect [28],[29]. In order to achieve the Scheimpflug condition, an adapter is used between the lens and the camera. The function of the adapter is to tilt the lens so that the film plane, lens plane and focus plane will intersect. Note the slightly tilted lens in cameras 1 and 2.*

When the Scheimpflug condition is satisfied, the focus area becomes larger. Figure 4.2.2 shows the difference between the Scheimpflug condition and non-Scheimpflug condition.

Stereo-PIV Calibration

Calibration is an essential part of Stereo-PIV. It can correct the perspective effect from the angle displacement arrangement and ensure accurate results. The method used in this study for calibration is the mathematical registration method. This method required a calibration target (cartesian grid of small dots) at the measurement plane. The image of the calibration target will be used to determine the magnification matrices and the

(a) *Scheimplug condition* (b) *non-Scheimplug condition*

Figure 4.2.2: *The difference between the Scheimpflug condition and non-Scheimpflug condition [22]. Note the larger in-focus area for the Scheimpflug condition.*

mapping functions [26]. Figure 4.2.3 shows the set-up of the calibration with the calibration plate.

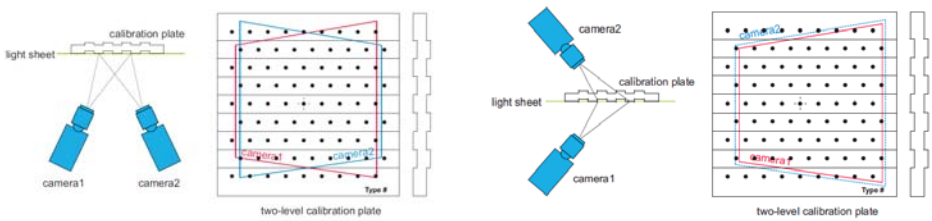

(a) *Forward Backward scattering* (b) *Forward Forward or Backward Backward scattering*

Figure 4.2.3: *Stereo-PIV calibration setup using calibration plate [22]*

Stereo-PIV Self Calibration

Self-calibration is a technique to compensate for the misalignment between the calibration plate and the light sheet. This extra calibration provides very accurate mapping functions. Details on the derivation in the self calibration technique can be found in [30] and [22]. Figure 4.2.4 shows the comparison with and without the self-calibration. The figure shows that, with the self-calibration, the disparity vectors can be reduced to zero.

Stereo-PIV Vector Calculation

The principle of extracting the velocity vector from stereo-PIV measurement is the same as in planar PIV. The difference is found before the cross-correlation is done; the images have to be dewarped first. This is because the raw image will suffer from the perspective error, and this must be corrected (dewarped) before the cross-correlation can be done. Details on dewarping can be found in [19].

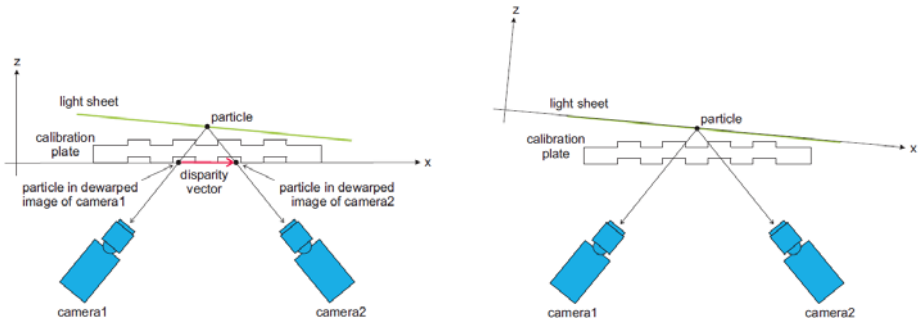

(a) *Without self calibration* (b) *With self calibration*

Figure 4.2.4: *Comparison before and after self calibration [22]*

Stereo-PIV in Liquid Flow

An extra device called liquid prism is needed for stereo-PIV measuerement in liquid flow. Liquid prism is a thin wall prism container filled with the same liquid as in the flow, which is then attached to the flat wall of the test section [25]. The function of liquid prism is to ensure an orthogonal view for the camera and reduce radial distortions arising from a liquid-air interface [27]. Figure 4.2.5 shows the set-up of stereo-PIV measurements with liquid prism.

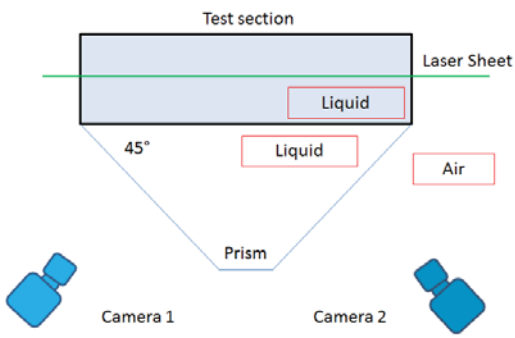

Figure 4.2.5: *Stereo PIV setup with liquid prism*

5 Torque Measurement

This chapter deals with torque measurements of the FZG gear, the FZG pinion, the cylinder gear, and the cylinder pinion. Several combinations of pairs and oil levels have been measured. Three different oil levels based on the test gear geometry have been applied in the measurements. Torque measurements were done using a torque meter that is mounted between the drive belt and the test section. With this arrangement, the torque is measured always from one side only, depending on the side on which it is mounted. If the torque meter is on the gear side, it will measure the torque from the gear only. If the torque meter is on the pinion side, it will measure the torque from the pinion only. Figure 5.0.1 shows a schematic of the oil level and the location of the torque meter on the rig.

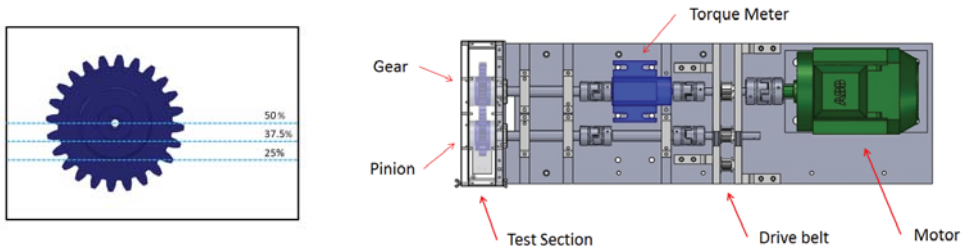

(a) *Oil level* (b) *Torque meter location*

Figure 5.0.1: *Oil level and location of the torque meter*

5.1 Aeration effect on torque measurement

The presence of air in the lubricant is called aeration. Figure 5.1.1 shows a comparison between aerated and non-aerated oil sump.

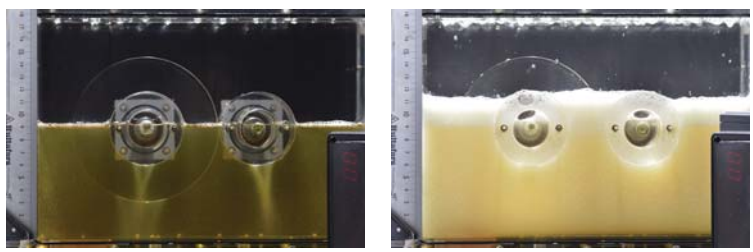

(a) *Non-aerated* (b) *Aerated*

Figure 5.1.1: *Comparison of non-aerated and aerated oil sump. Note the froth thickness as a result of aeration.*

In the present study, the aeration in the oil sump occurs due to the rotation of the gears. The higher the rotational speed, the higher the rate of bubble generation. The amount of aeration inside the test section can be estimated by measuring the froth height and then dividing by the initial oil level height. In this measurement, the amount of aeration inside is estimated to be 15 - 20%. In order to study the effect of aeration on the torque, three low RPM cases (150, 200, 250) was chosen. At these low RPM, the aeration inside the oil is considered minor and can be chosen as a base line. Figure 5.1.2 shows the results.

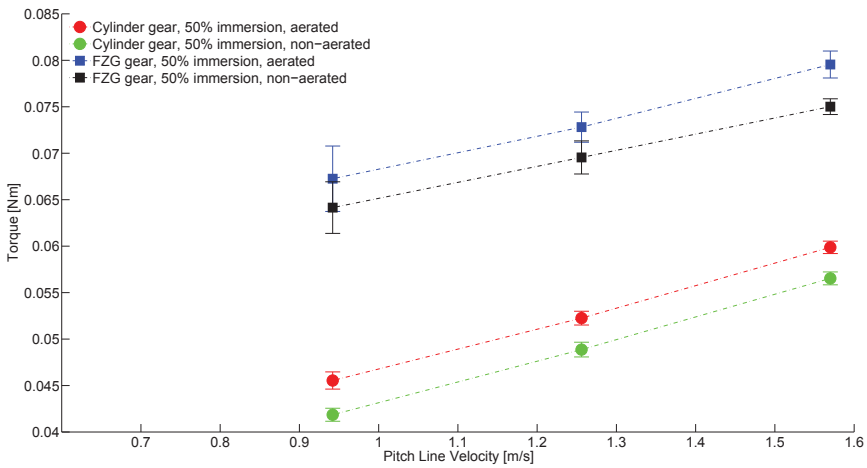

Figure 5.1.2: *Comparison of torque data of the single FZG gear and single cylinder gear with and without aeration*

The present study measures an increase of about 5-9% in the torque reading with aerated oil. The increase in torque is agrees with a previous study by [31]. They studied the effect of aeration at high rotational speed (4000 and 6000 RPM) and suggested that the reason for increasing torque is the additional energy that is needed to agitate and split the bubbles inside the test section. Another aeration study at lower RPM was done by [32]. The study suggested that the aeration alters the properties of the oil (in this case the viscosity), and the torque therefore increases.

Aeration takes place when the air is entrained and is trapped in the oil. Detailed studies of the mechanism of air entrainment to the liquid can be found in [33] and [34]. Unfortunately, stopping air from entraining into the oil sump is impossible. This is because the rotation of the gear always creates a void and a low pressure region between the teeth when the gear is rotating. Air will consequently entrain the oil, resulting in an air bubble. Inside the oil sump, the air bubble is drawn axially and ejected radially [35].

Aeration is a serious issue according to [36]. Aeration can generate heat by adiabatic compression of air bubbles. From a gear perspective, aerated oil also acts as an insulator, therefore reducing the conductivity from the gear to the oil. Hence, the temperature of

the oil increases. Another drawback is that aerated oil needs more energy to be pumped because the compressibility of air makes the oil flow rate only a fraction of what the pump normally supplies without aeration. The air bubble which are built up in the froth have a dampening effect, which retards the travel of the oil. The foam retards the oil travel through the air, resulting in failure to reach the critical zone in the machine, including bearing and gears.

In summary, the aeration increases the heat and the losses, although aeration is inevitable. The torque measurement data presented in this study have therefore all been measured in aerated oil.

5.2 Single gear measurements

In single gear measurements, the torque of the FZG gear, the FZG pinion, the cylinder gear and the cylinder pinion are measured individually. These data are then compared with the pair measurement torque in Section 5.3.

5.2.1 Single FZG gear and single cylinder gear torque

Figure 5.2.1 shows the torque of the single FZG gear and single cylinder gear measurement. It is seen that the resulting torque from the FZG gear and from the cylinder gear is essentially different.

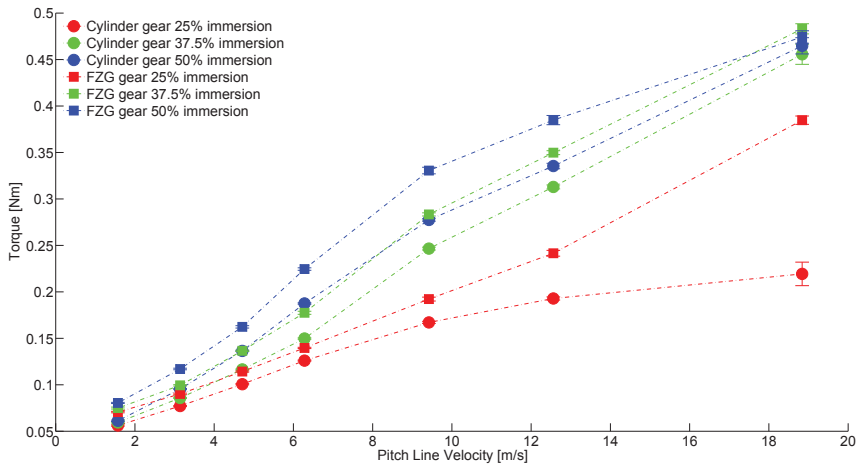

Figure 5.2.1: *Torque of the FZG gear and the cylinder gear with different oil levels and pitch line velocities*

Comparing the same immersion depth, the FZG gear has a higher torque reading compared to the cylinder gear at all pitch line velocities, except at the highest pitch line velocity. At a pitch line velocity of 18.84 m/s, the FZG gear and the cylinder gear with

37.5 and 50 % immersion depth, resulting in a little difference in the torque (2%). There is a significantly different torque (75% difference) for a 25% immersion depth between the FZG gear and the cylinder gear at the highest pitch line velocity. Although the cylinder gear has the same tip diameter as the FZG gear, the torque results suggest that gear teeth affect the torque.

5.2.2 Single FZG pinion and single cylinder pinion torque

Figure 5.2.2 shows the results of the torque measurement in the FZG pinion. The torque from the FZG pinion and the cylinder pinion are small compared to the FZG gear and the cylinder gear (approximately 50%). It can be concluded that the FZG gear is the dominant contribution to losses from the pair. According to the analysis in [37], [38], and [39], the gear geometry is a very important parameter in the churning losses, especially the radius. The larger the radius, the more drag is experienced by the gear and therefore the higher torque reading.

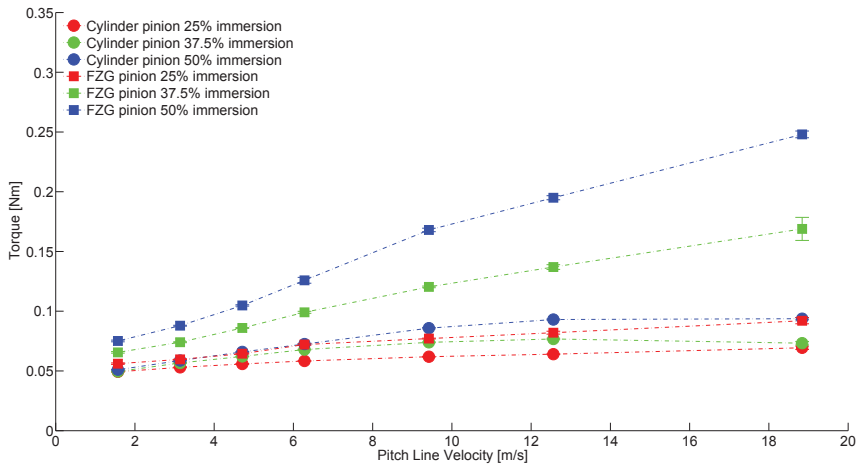

Figure 5.2.2: *Torque of the test pinion and the cylinder pinion with different oil levels and pitch line velocities*

5.3 Gear pair measurement

The previous section (Section 5.2) showed the torque from each individual gear. This section shows the effect of additional gears to the torque reading on each side.

5.3.1 Torque measurement on the gear side

Measurements were made on the gear side to check whether there is additional torque on the gear due to the presence of smaller gears. The measurements were made at immersion depths of 37.5 % and 50%. At an immersion depth of 25%, the cylinder pinion barely touches the surface of the oil. Torque at this immersion will therefore not be studied because the torque on the gear side is expected to be the same as in single gear measurement.

Figure 5.3.1 shows that the presence of the cylinder pinion affects the torque reading on the gear side. The presence of the cylinder pinion increases the torque reading. The torque difference at the highest pitch line velocity is 28% for the FZG gear and 18% for the cylinder gear at an immersion depth of 50%. The reason is that, at a certain pitch line velocity, the dragged oil is thick and detached from the cylinder pinion and showered to the gear. Hence, this effect increases the torque on the gear side.

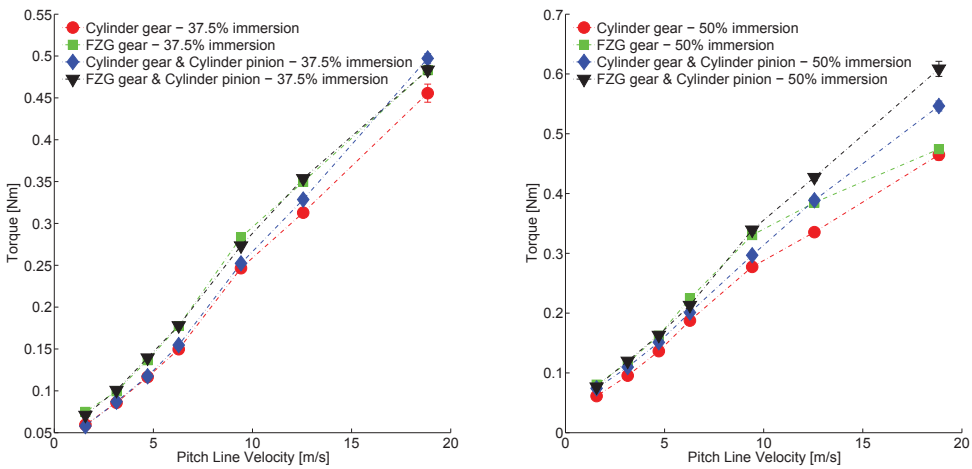

(a) *37.5% immersion* (b) *50% immersion*

Figure 5.3.1: *Comparison of torque measurement data on the gear side*

5.3.2 Torque measurement on the pinion side

Figure 5.3.2 shows the results of measurements on the pinion side. At the highest pitch line velocity, the results show that there is an increase of about 67% in the torque in the pinion due to the presence of the gear. On average, an increase of about 40% in the torque is experienced by the cylinder pinion when operating in the pair with the larger diameter gear. Another interesting phenomenon is that the cylinder pinion has higher losses when paired with the cylinder gear as compared to the test gear, especially at an immersion depth of 50%. This can be explained by the amount of dragged oil being different between the gear and cylinder. Gear teeth tend to throw the oil compared to the smooth cylinder surface, which drags the oil.

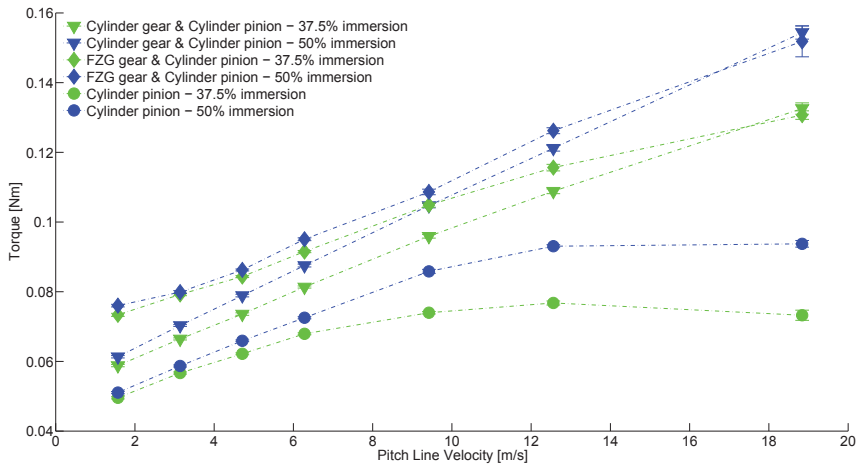

Figure 5.3.2: *Comparison of torque measurement on the pinion side*

6 Flow Visualization

This chapter deals with flow visualization of the oil flow inside the Chalmers rig. Two gear pairs are studied, the FZG gear type C and the cylinder gears. The oil level is at the centre line. The temperature of the oil is constant at 30°C. Comparisons of gear pair flow visualizations at different oil levels and different pitch line velocities can be seen in paper [40].

6.1 Flow visualization setup

For this study, a DSLR camera and a flash light Nikon D3200 and Nikon speedlight SB-700 are used. The camera is located in front of the test section and the flash is located at the top of the test section. Two reflectors are located on each side of the test section to fill the shadow region. Flash photography is fast enough to capture the instantaneous picture of the flow. With a flash duration at around 1/5000 sec in 1/8 of its maximum power, it is fast enough to freeze the splash that is created. Figure 6.1.1 shows the set-up of the lighting and camera.

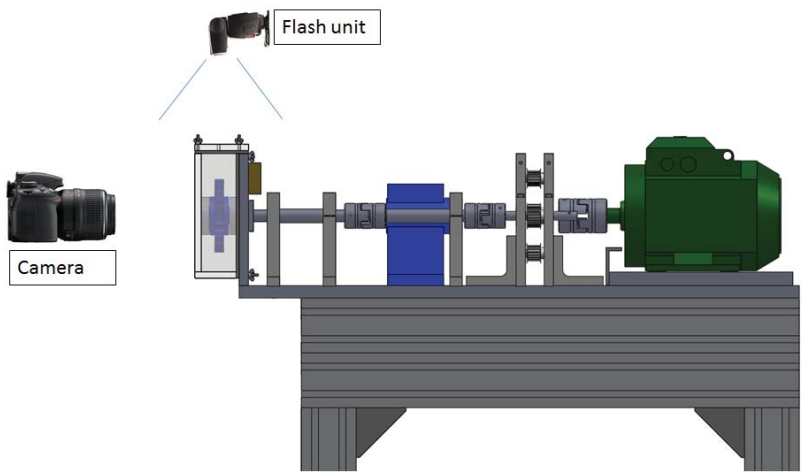

Figure 6.1.1: *The setup of the camera and the flash unit*

6.2 Visualization of single FZG gear and single cylinder gear

The purpose of single FZG gear and single cylinder gear flow visualization is to understand the flow inside the test section and to study how the single gear interact with the fluid

at different rotational speeds. Figure 6.2.1 shows a comparison between the single gear and single cylinder at rotational speeds of 50, 100, 150, 200, 250, and 300 RPM. It is seen that the bubble generation around the FZG gear is more prominent as compared to cylinder gear case. This is because some additional air is trapped in between the gear teeth and released into the oil sump. The bubbles in the cylinder gear case are from oil that is splashed into the oil sump and from air that is entrained due to the low pressure region close to the cylinder gear wall. The resulting flow feature for the cylinder is similar to that reported in a previous study by [41].

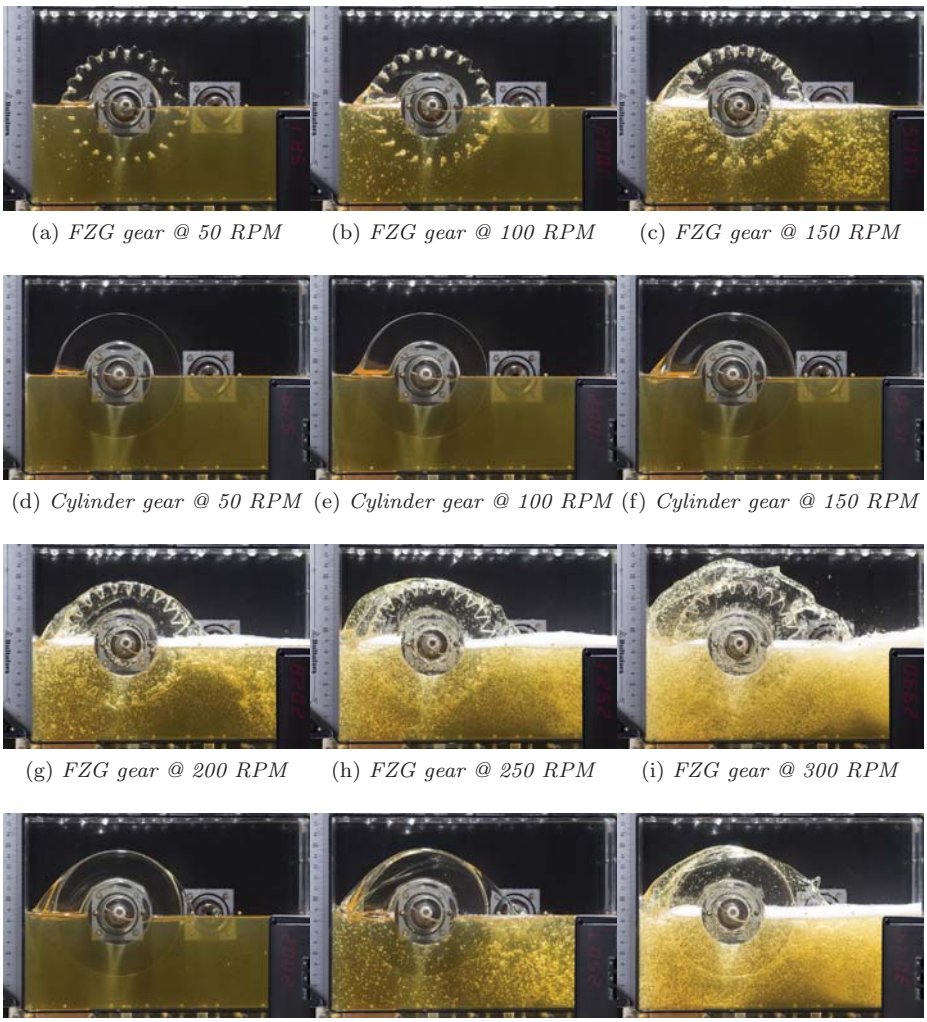

(a) *FZG gear @ 50 RPM* (b) *FZG gear @ 100 RPM* (c) *FZG gear @ 150 RPM*

(d) *Cylinder gear @ 50 RPM* (e) *Cylinder gear @ 100 RPM* (f) *Cylinder gear @ 150 RPM*

(g) *FZG gear @ 200 RPM* (h) *FZG gear @ 250 RPM* (i) *FZG gear @ 300 RPM*

(j) *Cylinder gear @ 200 RPM* (k) *Cylinder gear @ 250 RPM* (l) *Cylinder gear @ 300 RPM*

Figure 6.2.1: *Flow visualization of single FZG gear and single cylinder gear*

Figure 6.2.2 shows a comparison between single gear and single cylinder at rotational speeds of 350, 400, 450, 500, 550, and 600 RPM. At these rotational speeds, the inertia is large enough to detach oil from the gear body. The oil is thrown and detached from the body. The bubble generation increases with the rotational speed and obstructs the visibility.

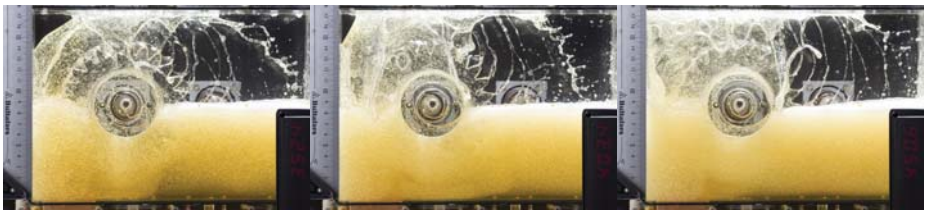

(a) *FZG gear @ 350 RPM* (b) *FZG gear @ 400 RPM* (c) *FZG gear @ 450 RPM*

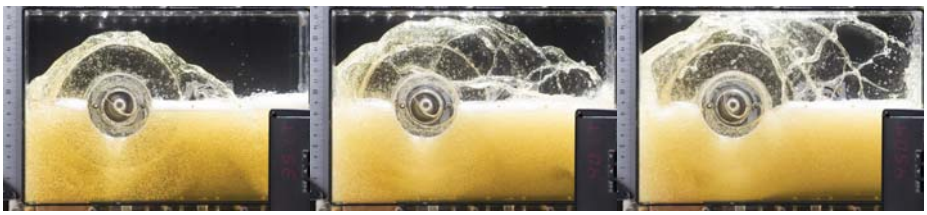

(d) *Cylinder gear @ 350 RPM* (e) *Cylinder gear @ 400 RPM* (f) *Cylinder gear @ 450 RPM*

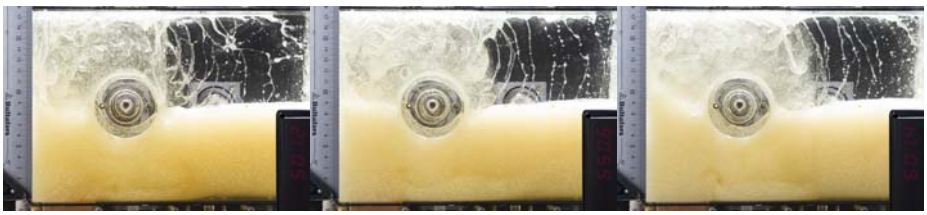

(g) *FZG gear @ 500 RPM* (h) *FZG gear @ 550 RPM* (i) *FZG gear @ 600 RPM*

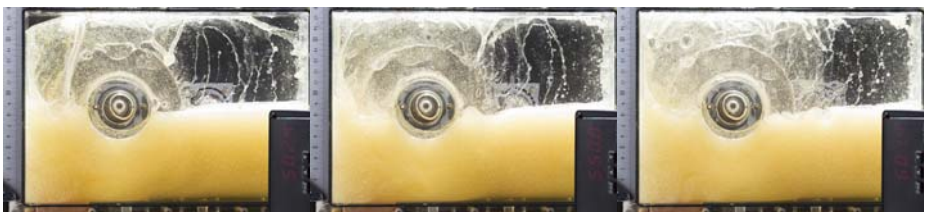

(j) *Cylinder gear @ 500 RPM* (k) *Cylinder gear @ 550 RPM* (l) *Cylinder gear @ 600 RPM*

Figure 6.2.2: *Flow visualization of single FZG gear and single cylinder gear*

6.3 Visualization of gear pair

This study was done in order to understand the flow interaction when the two gears rotate. Figure 6.3.1 shows a comparison of flow visualization between the FZG gear - cylinder pinion and cylinder pair. At a low rotational speed, the gear dragged oil upward and showered the pinion, adding torque to the pinion. The vice versa happens with a higher rotational speed.

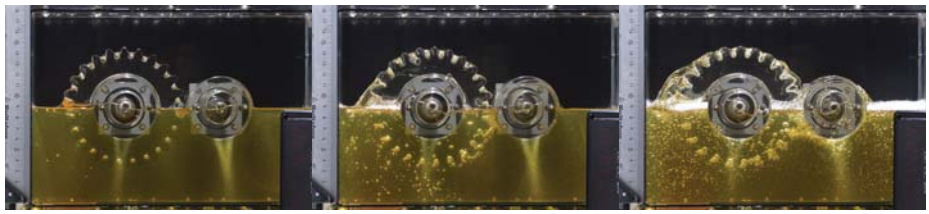

(a) *FZG gear - Cylinder pinion @ 50 RPM* (b) *FZG gear - Cylinder pinion @ 100 RPM* (c) *FZG gear - Cylinder pinion @ 150 RPM*

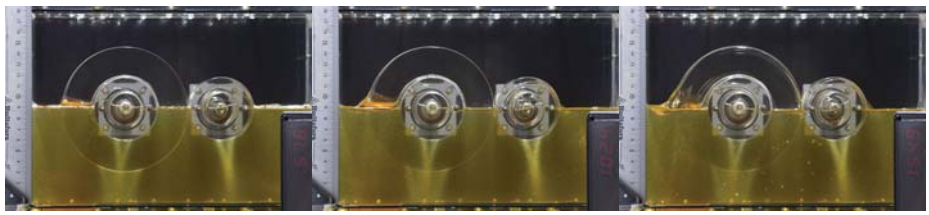

(d) *Cylinder pair @ 50 RPM* (e) *Cylinder pair @ 100 RPM* (f) *Cylinder pair @ 150 RPM*

(g) *FZG gear - Cylinder pinion @ 200 RPM* (h) *FZG gear - Cylinder pinion @ 250 RPM* (i) *FZG gear - Cylinder pinion @ 300 RPM*

(j) *Cylinder pair @ 200 RPM* (k) *Cylinder pair @ 250 RPM* (l) *Cylinder pair @ 300 RPM*

Figure 6.3.1: *Flow visualization of FZG gear - cylinder pinion and Cylinder pair*

Figure 6.3.2 shows a comparison between FZG gear - cylinder pinion and cylinder pair at rotational speeds of 350, 400, 450, 500, 550, and 600 RPM. At a very high rotational speed, the oil is mostly thrown to the side wall and the top wall, creating a void in the centre since the oil will flow to the front and back walls.

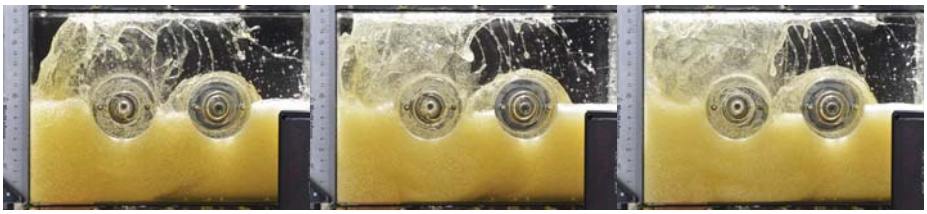

(a) *FZG gear - Cylinder pinion @ 350 RPM* (b) *FZG gear - Cylinder pinion @ 400 RPM* (c) *FZG gear - Cylinder pinion @ 450 RPM*

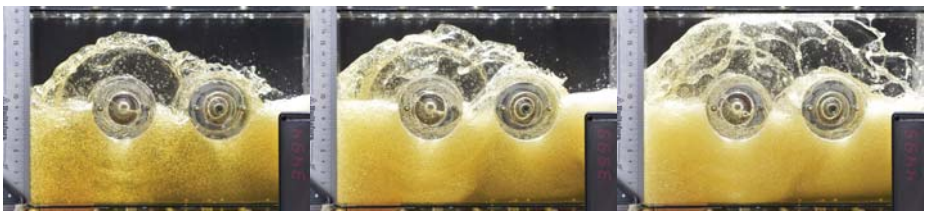

(d) *Cylinder pair @ 350 RPM* (e) *Cylinder pair @ 400 RPM* (f) *Cylinder pair @ 450 RPM*

(g) *FZG gear - Cylinder pinion @ 500 RPM* (h) *FZG gear - Cylinder pinion @ 550 RPM* (i) *FZG gear - Cylinder pinion @ 600 RPM*

(j) *Cylinder pair @ 500 RPM* (k) *Cylinder pair @ 550 RPM* (l) *Cylinder pair @ 600 RPM*

Figure 6.3.2: *Flow visualization of FZG gear - Cylinder pinion and cylinder pair*

7 Summary of Appended Papers

7.1 Paper A

E. A. Hartono, M. Golubev, and V. Chernoray. "PIV Study of Fluid Flow inside a Gearbox". In: *Proc. of 10th International Symposium on Particle Image Velocimetry* (2013), pp. 1–11

In paper *A*, flow visualization and PIV measurements of FZG gear pair type C were done. Three different oil levels (as seen in Figure 7.1.1) were measured; centre line, 2 module of pinion and 2 module of gear were tested. PIV measurement was done in the mid-plane of the test section. Full frontal view and zoom view below the gear and the pinion were shown. The generation of bubbles inside the gearbox set a limit to the PIV measurements. To get a good signal to noise ratio in the PIV measurement, the pitch line velocity was limited to 1.62 m/s. The PIV measurement reveals the flow structure at the mid-plane of the gearbox. The flow region is distinctly separated into two separated regions. This is shown by the stagnation region in the middle of the oil bath. PIV measurements also reveal that the flow structure of the test gear and test pinion is the same when the same immersion depth is applied.

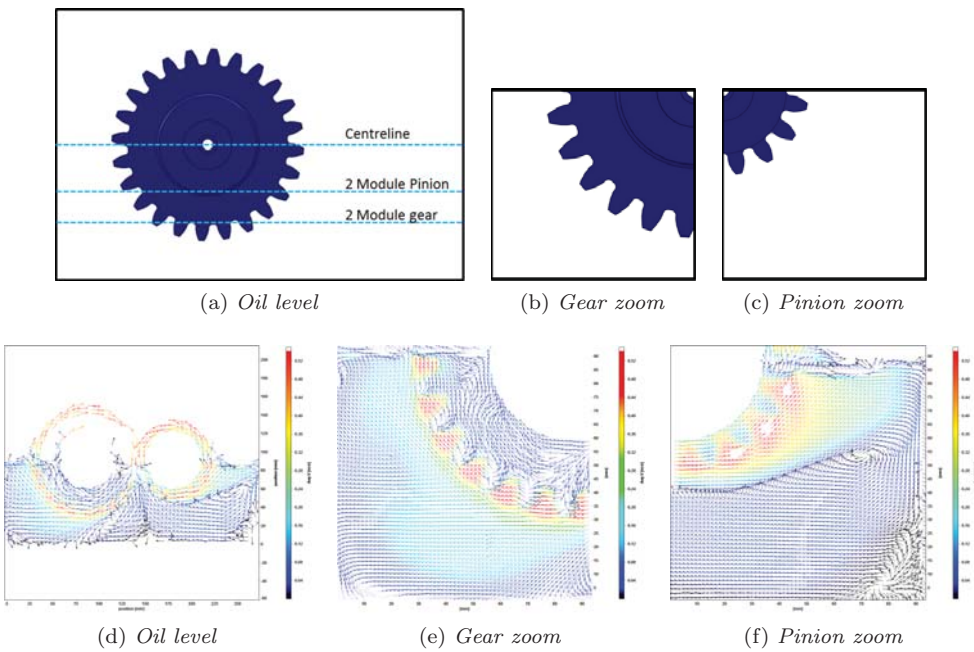

(a) *Oil level* (b) *Gear zoom* (c) *Pinion zoom*

(d) *Oil level* (e) *Gear zoom* (f) *Pinion zoom*

Figure 7.1.1: *Schematic of oil level and zoom view gear and pinion*

Some interesting flow features have been studied from flow visualizations. The larger

diameter gear governs the flow inside the gearbox. It is suspected that, because the larger diameter has a greater immersion depth, it draws up more oil and creates more splash, and also stirs the oil bath more. The deep immersion combined with a high rotational speed generates more bubbles. Rotation of the gear creates a low pressure region between the teeth and entrains air into the liquid. The air is trapped and various bubble sizes are formed. The faster the rotational speed, the larger the amount of air is trapped in between the teeth. The size of the trapped air bubbles reaches a maximum when the void in between the gear teeth is filled completely. After that point, the air bubbles which is bigger than the void will be cut by the gear teeth's edges and detach from the void. Figure 7.1.2 shows bubbles around the gear.

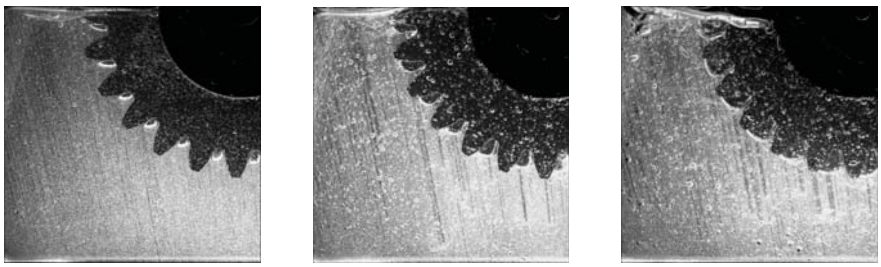

(a) *Vt = 0.55 m/s* (b) *Vt = 1.1 m/s* (c) *Vt = 1.62 m/s*

Figure 7.1.2: *Bubble around the gear at the centre line oil level*

Another feature in high rotational speed is the oil level change with the rotational speed. At a high rotational speed and centre line oil level, the changes in the oil line are more significant (around 15-20 mm).

(a) *Vt = 0.55 m/s* (b) *Vt = 2.64 m/s*

Figure 7.1.3: *Oil level drops due to high rotational speed*

7.2 Paper B

E. A. Hartono, A. Pavlenko, and V. Chernoray. "Stereo-PIV Study of Oil Flow inside a Model Gearbox". In: *Proc. of 17th International Symposium on Applications of Laser Techniques to Fluid Mechanics* (2014), pp. 1–8

The work reported in this paper made measurements of stereo-PIV. Stereo-PIV can capture the third components of the flow. The results suggest that the oil flow inside the gearbox is indeed three dimensional. Stereo-PIV was also done in the gear contact region to check the squeezing of fluid in gear contact. For this case, to study the squeezing in detail, the gearbox is filled completely with oil and the ejection velocity is measured.

The flow pattern at the mid-plane is acquired from planar PIV. The flow pattern at the cross plane is acquired from the stereo PIV. Figure 7.2.1 shows the schematic of the recirculation in three planes (X,Y,Z) and the final three dimensional streamlines of the flow. The three dimensional streamlines are a result of combining stereo-PIV data from 5 planes along the axis. The three dimensional streamlines are similar to those reported in previous study [41].

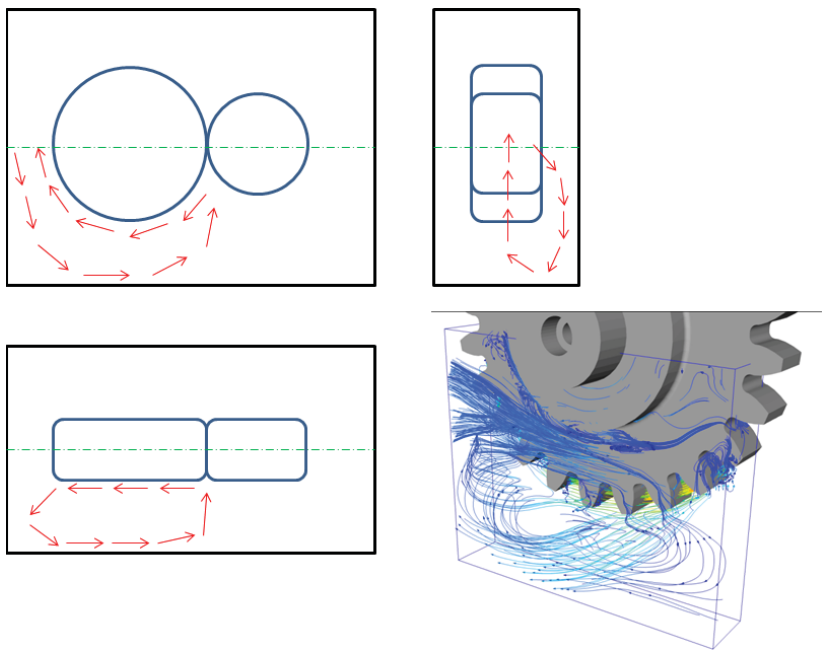

Figure 7.2.1: *Stereo-PIV measurement results and visualization of recirculation region*

Figure 7.2.2 shows the results of stereo PIV measurements below the gear axis. The figure shows that there are two recirculation regions. It is seen that the size of the high speed region is closer to the gear teeth when the rotational speed is higher. The recirculation is also stronger compared to the low rotational speed case. This strong

recirculation is most probably what contributes to increasing churning losses.

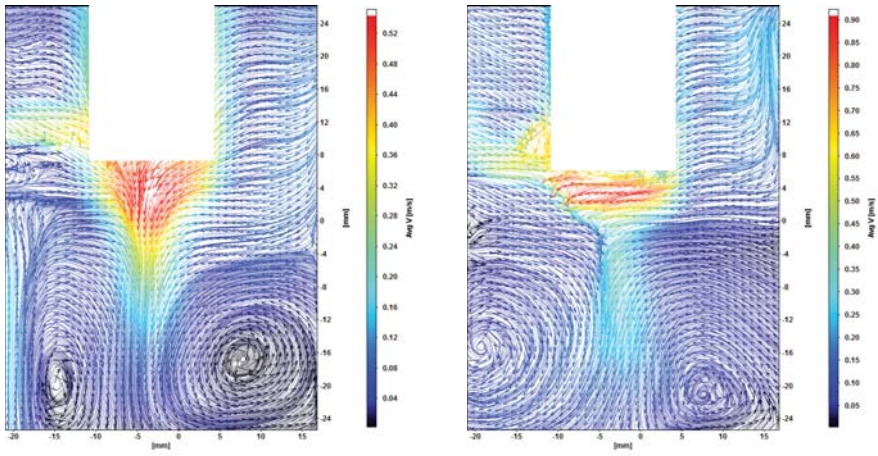

(a) $Vt = 0.55m/s$ (b) $Vt = 1.10m/s$

Figure 7.2.2: *Stereo-PIV of cross flow below the gear axis*

At gear contact, oil squeezing is the main concern because it creates losses. These losses are measured by making PIV measurements in the gear contact plane to check the velocity of ejecting fluid from the gear teeth. The results show that the mass flow is small compared to the recirculation, so the losses from the squeezing effect are rather small, considering that the oil level in the real geometry is lower than at the centre line. Figure 7.2.3 shows the velocity fields at the gear contact.

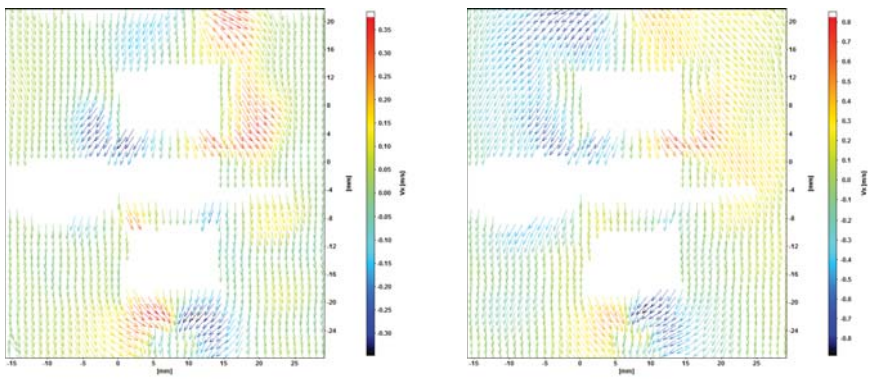

(a) $Vt = 0.55m/s$ (b) $Vt = 1.10m/s$

Figure 7.2.3: *Stereo-PIV of cross flow below the gear axis*

8 Conclusions

8.1 Concluding Remarks

The Chalmers gearbox flow facility gives a solid foundation for further research in oil flow inside a gearbox. The facility is versatile and can easily be modified. The structure is quite solid for handling the workload, and the torque measurements can thus be made with good accuracy.

The flow visualization method produced good insight into the flow distribution in the test section. The method is successful and can be implemented or even extended with the use of a faster shutter speed camera combined with a faster flash rate.

PIV measurements measured the velocity fields of the oil. The measurements were made for different oil levels and different rotational speeds. The data can be directly compared with numerical simulations. The data have a good signal to noise ratio due to a low rotational speed. The method is successful and can be improved for measuring at higher rotational speeds.

In summary, the database for numerical validation has been acquired and these data can be easily reproduced or improved.

8.2 Future Work

The future of this study will first be numerical studies, since experimental data have been gathered. The study will try to investigate the possibility of modifying gear geometry in a plain cylinder. If successful, the savings in computational time will be significant, since there is no gear contact and no zero mesh size.

Future work will also investigate the oil flow inside the gearbox with modified housing, as previous studied [43]. This study suggests that housing can influence the churning losses. This method gives good opportunities to reduce the losses since the gear geometry cannot be altered due to mechanical design requirements. The inner wall of the housing will therefore need to be modified in order to guide the flow and redirect it to the hot spot.

For torque measurements, the torque from real transmission oil will be measured and compared with the existing torque data. This is because the real transmission oil has additives, one of the additives being to decrease aeration by making the bubbles break up easily. The torque measurement will assess the capability of this additive.

Vertical configuration and heat transfer will be studied, as will be a step closer to the real transmission unit. The end goal of this study is to find the minimum amount of oil that gives the least amount of losses without compromising the lifetime of the gear.

References

[1] K. Holmberg et al. “Global Energy Consumption due to Friction in Trucks and Buses”. In: *Tribology International* 78 (2014), pp. 94–114.

[2] K. Holmberg, P. Andersson, and A. Erdemir. “Global Energy Consumption due to Friction in Passenger Cars”. In: *Tribology International* 47 (2011), pp. 221–234.

[3] M. Dahlbäck. personal communication. Oct. 13, 2014.

[4] A. S. Kolekar et al. “Windage and Churning Effects in Dipped Lubrication”. In: *Journal of Tribology* 136 (2014), pp. 021801–1–021801–10.

[5] H. P. Otto. “Flank Load Carrying Capacity and Power Loss Reduction by Minimised Lubrication”. PhD thesis. Technische Universität Munchen, 2009.

[6] B.-R. Höhn, K. Michaelis, and H.-P. Otto. “Influence of Immersion Depth of Dip Lubricated Gears on Power Loss, Bulk Temperature and Scuffing Load Carrying Capacity”. In: *Int J Mech Mater Des* 4 (2008), pp. 145–156.

[7] B.-R. Höhn, K. Michaelis, and H.-P. Otto. “Minimised Gear Lubrication by a Minimum Oil/Air Flow Rate”. In: *Wear* 266 (2008), pp. 461–467.

[8] M. F. Ashby and D. R. H. Jones. *Engineering Materials*. Butterworth-Heinemann, 1998. ISBN: 0-7506-4019-7.

[9] “Lubrication Basics”. In: *Machinery Lubrication* April (2010).

[10] J. DeBaecke. “Understanding and Maintaining an Effective Lubrication System”. In: *Hydrocarbon Processing* Aug (2009), pp. 27–33.

[11] M. J. Neale. *The Tribology Handbook*. Elsevier, 1995. ISBN: 978-0-7506-1198-5.

[12] *1996 Land Rover Discovery Manual Gearbox @AutoPartsLIB.com*. 2009. URL: `http://www.autopartslib.com/1996-land-rover-discovery-manual-gearbox-assembly-parts-diagram/`.

[13] G. Leprince et al. “Investigations on Oil Flow Rates Projected on the Casing Walls by Splashed Lubricated Gears”. In: *Advances in Tribology* 2012 (2012), pp. 1–7.

[14] E. G. Ellis. “Fundamentals of Lubrication”. In: *Industrial Lubrication* February (1967), pp. 63–69.

[15] I. Grant. “Particle Image Velocimetry: A Review”. In: *Proc Instn Mech Engrs* 211 part C (1997), pp. 55–76.

[16] C. E. Willert and M. Gharib. “Digital Particle Image Velocimetry”. In: *Experiments in Fluids* 10 (1991), pp. 181–193.

[17] R. J. Adrian. “Twenty Years of Particle Image Velocimetry”. In: *Experiments in Fluids* 39 (2005), pp. 159–169.

[18] R. J. Adrian and J. Westerweel. *Particle Image Velocimetry*. Cambridge, 2011. ISBN: 978-0-521-44008-0.

[19] M. Rafell et al. *Particle Image Velocimetry - A Practical Guide*. Springer, 2007. ISBN: 978-3-540-72307-3.

[20] *Flow Master Getting Started*. LaVision. 2014.

[21] *LaVision PIV Illustration*. 2014. URL: `http://www.lavision.de/en/downloads/poster.php`.

[22] *Flow Master Product Manual*. LaVision. 2014.

[23] A. Melling. “Tracer Particles and Seeding for Particle Image Velocimetry”. In: *Meas. Sci. Technol.* 8 (1997), pp. 1406–1416.
[24] C. Tropea, A. L. Yarin, and J. F. Foss. *Springer Handbook of Experimental Fluid Mechanics*. Springer, 2007. ISBN: 978-3-540-25141-5.
[25] A. K. Prasad and K. Jensen. “Scheimpflug Stereocamera for Particle Image Velocimetry in Liquid Flows”. In: *Applied Optics* 34 (1995), pp. 7092–7099.
[26] S. Zhang. *Handbook of 3D Machine Vision - Optical Metrology and Imaging*. Taylor and Francis, 2013. ISBN: 978-1-4398-7220-8.
[27] A. Prasad and R. Adrian. “Stereoscopic Particle Image Velocimetry Applied to Liquid Flows”. In: *Experiments in Fluids* 15 (1993), pp. 49–60.
[28] H. M. Merklinger. “View Camera Focus and Depth of Field - Part 1”. In: *View Camera Magazine* July/August (1996), pp. 55–57.
[29] H. M. Merklinger. “View Camera Focus and Depth of Field - Part 2”. In: *View Camera Magazine* September/October (1996), pp. 56–58.
[30] B. Wieneke. “Stereo-PIV using Self-Calibration on Particle Images”. In: *Experiments in Fluids* 39 (2005), pp. 297–280.
[31] G. Leprince et al. “Influence of Aerated Lubricants on Gear Churning Losses - An Engineering Model”. In: *Tribology Transactions* 54 (2011), pp. 929–938.
[32] A. T. J. Hayward. “Research on Lubricants and Hydraulic Fluids at the National Engineering Laboratory”. In: *Industrial Lubrication and Tribology* 15 (1963), pp. 112–124.
[33] X. Qu et al. “Experimental Characterization of air-entrainment in a plunging jet”. In: *Experimental Thermal and Fluid Science* 44 (2012), pp. 51–61.
[34] W. K. Soh et al. “The Entrainment of Air by Water Jet Impinging on A Free Surface”. In: *Experiments in Fluids* 39 (2005), pp. 496–504.
[35] P. H. Dawson. “Windage Loss in Larger High Speed Gears”. In: *Proc Instn Mech Engrs* 198A (1984), pp. 51–59.
[36] J. Fitch. “The Perils of Aerated Oil - Let Your Machine Burp”. In: *Practicing Oil Analysis* 1 (2005).
[37] C. Changenet et al. “A Note on Flow Regimes and Churning Loss Modelling”. In: *Journal of Mechanical Design* 133 (2011), pp. 121009–1–121009–5.
[38] R. J. Boness. “Churning Losses of Discs and Gears Running Partially Submerged in Oil”. In: *Proceedings of the 1989 International Power Transmission and Gearing Conference* 1 (2009), pp. 355–359.
[39] S. Seetharaman et al. “Oil Churning Power Losses of a Gear Pair: Experiments and Model Validation”. In: *Journal of Tribology* 131 (2009), pp. 022202–1–022202–10.
[40] E. A. Hartono, M. Golubev, and V. Chernoray. “PIV Study of Fluid Flow inside a Gearbox”. In: *Proc. of 10th International Symposium on Particle Image Velocimetry* (2013), pp. 1–11.
[41] M. S. Christodoulou, J. T. Turner, and S. D. R. Wilson. “Experimental Study and Improvement of the Rotating Disc Skimmer”. In: *IOSC Proceedings* 1 (1987), pp. 101–108.
[42] E. A. Hartono, A. Pavlenko, and V. Chernoray. “Stereo-PIV Study of Oil Flow inside a Model Gearbox”. In: *Proc. of 17th International Symposium on Applications of Laser Techniques to Fluid Mechanics* (2014), pp. 1–8.

[43] C. Chengenet and P. Velex. “Housing Influence on Churning Losses in Geared Transmissions”. In: *Journal of Mechanical Design* 130 (2008), pp. 062603–1–062603–6.